Nonperturbative renormalization of meson decay constants in quenched QCD for a renormalization group improved gauge action

doi: 10.1103/PhysRevD.70.074502

Nonperturbative renormalization of meson decay constants in quenched QCD for a renormalization group improved gauge action

K. Ide,[1] S. Aoki,[1] R. Burkhalter,[1,2,*] M. Fukugita,[3] S. Hashimoto,[4] K.-I. Ishikawa,[1,2,†] T. Ishikawa,[2] N. Ishizuka,[1,2] Y. Iwasaki,[1,2] K. Kanaya,[1] T. Kaneko,[4] Y. Kuramashi,[4,‡] V. Lesk,[2,§] M. Okawa,[5] Y. Taniguchi,[1] T. Umeda,[2,‖] A. Ukawa,[1,2] and T. Yoshié[1,2]

(CP-PACS Collaboration)

[1]*Graduate School of Pure and Applied Sciences, University of Tsukuba, Tsukuba, Ibaraki 305-8571, Japan*
[2]*Center for Computational Sciences, University of Tsukuba, Tsukuba, Ibaraki 305-8577, Japan*
[3]*Institute for Cosmic Ray Research, University of Tokyo, Tanashi, Tokyo 188-8502, Japan*
[4]*High Energy Accelerator Research Organization (KEK), Tsukuba, Ibaraki 305-0801, Japan*
[5]*Department of Physics, Hiroshima University, Higashi-Hiroshima, Hiroshima 739-8526, Japan*

(Received 6 May 2004; published 5 October 2004)

Renormalization constants (Z-factors) of vector and axial-vector currents are determined nonperturbatively in quenched QCD for a renormalization group improved gauge action and a tadpole-improved clover quark action using the Schrödinger functional method. Nonperturbative values of Z-factors turn out to be smaller than 1-loop perturbative values by $O(15\%)$ at a lattice spacing of $a^{-1} \approx 1$ GeV. The pseudoscalar and vector meson decay constants calculated with the nonperturbative Z-factors show a much better scaling behavior compared to previous results obtained with tadpole-improved one-loop Z-factors. In particular, the nonperturbative Z-factors normalized at infinite physical volume show that the scaling violations of the decay constants are within about 10% up to the lattice spacing $a^{-1} \sim 1$ GeV. The continuum estimates obtained from data in the range $a^{-1} \sim 1$–2 GeV agree with those determined from finer lattices ($a^{-1} \sim 2 - 4$ GeV) with the standard action.

DOI: 10.1103/PhysRevD.70.074502 PACS numbers: 12.38.Gc

I. INTRODUCTION

Reliable prediction of physical quantities from lattice QCD calculations requires a good control of scaling violations. For this purpose, several improved actions have been tested and applied to large scale systematic simulations. For most physical quantities, such as quark masses and hadronic matrix elements, one has to calculate in addition renormalization constants (Z-factors). Nonperturbative methods to determine various Z-factors have been developed and utilized for several actions.

The CP-PACS collaboration carried out systematic simulations for two-flavor full QCD [1] using a renormalization group (RG) improved gauge action [2] and a tadpole-improved [3] clover quark action [4] and reported results for the spectrum, quark masses and meson decay constants. Since nonperturbative Z-factors were not available for this action combination, the analysis had to rely on one-loop perturbative values. The result showed that the meson decay constants in both quenched and full QCD suffer from large scaling violations at $a^{-1} \sim 1 - 2$ GeV which hinder continuum extrapolations. It was not clear if this observation hinted at an inherent difficulty of improved actions for matrix elements at coarse lattice spacings or a perturbative treatment of the Z-factors was the issue. A nonperturbative determination of Z-factors was evidently needed.

As a first step toward a systematic study of nonperturbative renormalization for this action, we apply the Schrödinger functional (SF) method [5–8] to calculations of Z-factors for vector (Z_V) and axial-vector (Z_A) currents in quenched QCD with the same improved action. The SF method has been applied to the nonperturbatively $O(a)$ improved Wilson action. In contrast, our action combination has $O(ag^4)$ error, since the coefficient of the clover term is determined by tadpole-improved perturbation theory to one-loop order. Therefore our study involves an examination whether the SF method successfully works for this action

In the SF method, Z-factors are determined at various couplings for a fixed physical size L. In this case, the Z-factors contain terms of $O(ag^4/L)$ in addition to that of $O(a\Lambda)$. We expect that one can remove the $O(ag^4/L)$ terms by taking the infinite volume limit. We calculate Z-factors both at a finite fixed physical volume and at the

*Present address: Julius Baer Investment Fund Services Ltd., Freigutstrasse 12, 8010 Zurich, Switzerland
†Present address: Department of Physics, Hiroshima University, Higashi-Hiroshima, Hiroshima 739-8526, Japan
‡Present address: Center for Computational Sciences, University of Tsukuba, Tsukuba, Ibaraki 305-8577, Japan
§Present address: Department of Biological Sciences, Imperial College, London SW7 2AZ, United Kingdom.
‖Present address: Yukawa Institute for Theoretical Physics, Kyoto University, Kyoto 606-8502, Japan

infinite volume and compare the scaling properties of decay constants with these two choices of Z-factors.

When we calculate Z-factors for large couplings and on large lattices, we encounter "exceptional configurations" for which observables take abnormally large values. We estimate systematic uncertainties due to such configurations, propagate them to systematic error estimations of decay constants, and argue that they do not alter our conclusions on scaling properties.

The organization of this paper is as follows. In Sec. II we describe calculation method focusing on features of applying the SF method to the RG-improved action. Details of the analysis for Z_V and Z_A are given in Sec. III. With these Z-factors, we study the scaling behavior of decay constants of vector (f_ρ) and pseudoscalar (f_π) mesons in Sec. IV. Sec. V is devoted to conclusions. Parts of this work have already been reported in Refs. [9,10].

II. CALCULATION METHOD

A. Action and Currents

The RG-improved gauge action we employ has the form

$$S_g = \frac{\beta}{6}\left\{c_0 \sum_{x,\mu,\nu} U_{P,\mu\nu}(x) + c_1 \sum_{x,\mu,\nu} U_{R,\mu\nu}(x)\right\}, \qquad (1)$$

where $\beta = 6/g^2$ with the bare coupling constant g, and U_P (U_R) is the trace of the product of link variables around a plaquette (6-link rectangular loop). In a sum over loops, each oriented loop appears once. The coefficients $c_1 = -0.331$ and $c_0 = 1 - 8c_1 = 3.648$ are fixed by an approximate RG analysis [2].

The clover quark action [4] is defined by

$$S_q = \sum_{x,y} \overline{\psi}(x) D_{x,y} \psi(y), \qquad (2)$$

$$D_{x,y} = \delta_{x,y} - \kappa \sum_{\mu} \{(1-\gamma_\mu) U_{x,\mu} \delta_{x+\hat{\mu},y} + (1+\gamma_\mu) U^\dagger_{x,\mu} \delta_{x,y+\hat{\mu}}\} - \delta_{x,y} c_{SW} \kappa \sum_{\mu<\nu} \sigma_{\mu\nu} F_{\mu\nu}, \qquad (3)$$

where κ is the hopping parameter and $F_{\mu\nu}$ is a lattice discretization of the field strength. For the clover coefficient c_{SW}, we adopt a tadpole-improved value with one-loop estimate of the plaquette $\langle W^{1\times1}\rangle = \frac{1}{3}\langle U_{P,\mu\nu}\rangle$ given by

$$c_{SW} = \langle W^{1\times1}\rangle^{-3/4} = (1 - 0.8412/\beta)^{-3/4}, \qquad (4)$$

since we use the one-loop value of the plaquette reproduces measured values well.

For Z_V, we investigate the vector Ward identity of the unimproved current V^a_μ since the particular SF setup we use yields the same value of Z_V for improved and unimproved currents. On the other hand, we study an improved current for Z_A defined by

$$(A_I)^a_\mu(x) = A^a_\mu(x) + a c_A \frac{1}{2}(\partial^*_\mu + \partial_\mu) P^a(x), \qquad (5)$$

where ∂^*_μ and ∂_μ are lattice forward and backward derivatives and $P^a(x)$ is the pseudoscalar density. We use the one-loop value for the improvement coefficient $c_A = -0.0038 g^2$ [11].

B. Implementation for RG-Improved Action

We follow the SF method of Ref. [8] for the RG-improved gauge action. Taking an $L^3 \times T$ lattice, we impose the periodic boundary condition in the spatial directions and the Dirichlet boundary condition in the temporal direction.

The boundary counter terms for the RG-improved action are determined [12] so that the classical field equations are satisfied. The total action reads

$$S_g = \frac{\beta}{6} \sum_{\mathbf{x}} \sum_{x_4=0}^{T} \left\{ c_0 \sum_{\mu,\nu} w^P_{\mu\nu}(x_4) U_{P,\mu\nu}(x) + c_1 \sum_{\mu,\nu} w^R_{\mu\nu}(x_4) U_{R,\mu\nu}(x) \right\}, \qquad (6)$$

with the weight factors $w^P_{\mu\nu}(x_4)$ and $w^R_{\mu\nu}(x_4)$ given by

$$w^P_{\mu\nu}(x_4) = \begin{cases} c_t & (x_4 = 0 \quad \text{or} \quad x_4 = T - a) \quad \text{and} \quad (\mu = 4 \quad \text{or} \quad \nu = 4) \\ 0 & x_4 = T \quad \text{and} \quad (\mu = 4 \quad \text{or} \quad \nu = 4) \\ \frac{1}{2} c_s & (x_4 = 0 \quad \text{or} \quad x_4 = T) \quad \text{and} \quad (\mu \neq 4 \quad \text{and} \quad \nu \neq 4) \\ 1 & \text{otherwise.} \end{cases} \qquad (7)$$

$$w^R_{\mu\nu}(x_4) = \begin{cases} \frac{3}{2} & \text{when 2 links of the rectangular touch a boundary} \\ 0 & \text{when the rectangular is completely included in an boundary} \\ 1 & \text{otherwise.} \end{cases} \quad (8)$$

We take the tree-level value of $c_s = c_t = 1$. (One-loop values of c_s and c_t [13] were not known when we started this work.) Boundary counter terms are not included for the clover quark action. In other words, the boundary coefficients $\tilde{c}_s$ and $\tilde{c}_t$ of Ref. [8] are set to the tree-level values, $\tilde{c}_s = \tilde{c}_t = 1$.

C. Details of Calculation Method

We calculate Z-factors for the range $\beta = 8.0 - 2.2$. The smallest value $\beta = 2.2$ is chosen to lie in the range $\beta = 2.575 - 2.184$ (inverse lattice spacing $a^{-1} \approx 1 - 2$ GeV) where data for f_ρ and f_π exist [1]. Simulations are made with a 5-hit pseudo-heat-bath algorithm mixed with an over-relaxation algorithm in the ratio of 1:4. We analyze 200 – 20000 configurations separated by 100 sweeps each. The lattice geometry is set to $T = 2L$ for both Z_V and Z_A. At each β, Z-factors are determined for at least two lattice sizes in order to interpolate or extrapolate them to a fixed physical volume. Lattice size and number of analyzed configurations are listed in Table I.

Calculations of Z-factors are carried out at zero quark mass, where the quark mass m_q is defined by the PCAC relation $\partial_\mu A^a_\mu = 2m_q P^a$ in the continuum notation. The actual procedure to measure m_q is the same as in Ref. [7]. We define a time-dependent quark mass by

$$m_q(x_4) = \frac{\frac{1}{2}(\partial^*_0 + \partial_0) f_A(x_4) + c_A a \partial^*_0 \partial_0 f_P(x_4)}{2 f_P(x_4)}, \quad (9)$$

where f_A is the axial-vector and pseudoscalar correlator and f_P is the pseudoscalar and pseudoscalar correlator. The quark mass m_q is defined by an average of $m_q(x_4)$ over a range of time slices around $x_4 = T/2$;

$$m_q = \frac{1}{2n+1} \sum_{t=-an}^{an} m_q\left(\frac{T}{2} + t\right), \quad (10)$$

where n defines the range and depends on simulation parameters.

Z-factors are determined from correlators of pseudoscalar operators P^a and P'^a at the boundaries and/or currents V^a_μ and $(A_I)^a_\mu$ at a finite time slice. We employ the notations defined by

$$f_1 = -\frac{1}{3L^6} \langle P'^a P^a \rangle, \quad (11)$$

$$f_V(x_4) = \frac{a^3}{6L^6} \sum_{\mathbf{x}} i\epsilon^{abc} \langle P'^a V^b_0(x) P^c \rangle, \quad (12)$$

TABLE I. Simulation parameters and Z-factors at simulation points. For $8^3 \times 16$ lattices at $\beta = 2.2$ and 2.4 where we encounter exceptional configurations, we quote only central values and statistical errors. No calculations of Z_A were made for $16^3 \times 32$ lattice at $\beta = 2.8$ and $12^3 \times 24$ lattice at $\beta = 8.0$.

β	$L^3 \times T$	κ_c	m_q	Z_V	#conf for Z_V	Z_A	#conf for Z_A
2.2	$4^3 \times 8$	0.139 281(56)	-0.000 529(495)	0.7499(11)	2000	0.7667(52)	2000
	$8^3 \times 16$	0.140 570(15)	0.001 493(399)	0.7067(12)	20 000	0.7350(610)	20 000
2.4	$4^3 \times 8$	0.136 933(21)	-0.000 764(337)	0.7995(10)	1000	0.8150(24)	2000
	$8^3 \times 16$	0.137 481(04)	-0.000 130(395)	0.7652(04)	10 000	0.7525(204)	10 000
2.6	$4^3 \times 8$	0.135 558(08)	-0.000 276(341)	0.8265(05)	2000	0.8474(16)	2000
	$8^3 \times 16$	0.135 701(10)	-0.000 464(154)	0.8056(05)	500	0.8208(18)	2000
2.8	$4^3 \times 8$	0.134 532(10)	0.000 002(396)	0.8482(06)	1000	0.8667(18)	1000
	$8^3 \times 16$	0.134 515(07)	-0.000 105(139)	0.8312(04)	500	0.8482(13)	1000
	$12^3 \times 24$	0.134 554(08)	0.000 525(111)	0.8268(03)	500	0.8520(17)	1000
	$16^3 \times 32$	0.134 587(09)	0.000 663(139)	0.8231(06)	500		
3.125	$12^3 \times 24$	0.133 209(01)	-0.000 039(091)	0.8540(02)	500	0.8689(09)	500
	$16^3 \times 32$	0.133 219(05)	-0.000 092(060)	0.8527(01)	500	0.8672(08)	500
4.0	$8^3 \times 16$	0.131 094(04)	-0.000 302(086)	0.8972(02)	500	0.9068(06)	500
	$16^3 \times 32$	0.131 083(01)	0.000 160(044)	0.8938(01)	500	0.9060(04)	300
6.0	$8^3 \times 16$	0.128 898(03)	-0.000 191(061)	0.9366(01)	300	0.9425(03)	300
	$16^3 \times 32$	0.128 891(01)	-0.000 060(023)	0.9337(01)	300	0.9398(02)	300
8.0	$8^3 \times 16$	0.127 869(02)	0.000 138(041)	0.9545(01)	300	0.9600(02)	300
	$12^3 \times 24$	0.127 870(01)	0.000 576(331)	0.9523(01)	300		
	$16^3 \times 32$	0.127 870(01)	0.000 021(017)	0.95151(3)	300	0.9565(01)	200

$$f_{AA}(x_4, y_4) = -\frac{a^6}{6L^6}\sum_{\mathbf{x},\mathbf{y}} \epsilon^{abc}\epsilon^{cde}\langle P'^d (A_I)_0^a(x)(A_I)_0^b(y)P^e\rangle. \tag{13}$$

Renormalization constants are then extracted from

$$Z_V = \frac{f_1}{f_V(\frac{T}{2})}, \tag{14}$$

$$Z_A = \sqrt{\frac{f_1}{f_{AA}(\frac{3T}{8}, \frac{5T}{8})}}. \tag{15}$$

The lattice spacing necessary to set the physical size is determined from the string tension $\sqrt{\sigma} = 440$ MeV. We fit values of $a\sqrt{\sigma}$ [1,14] to a fitting form [15]

$$(a\sqrt{\sigma})(\beta) = f(\beta)[1 + c_2\hat{a}^2(\beta) + c_4\hat{a}^4(\beta) + \cdots]/c_0,$$
$$\hat{a}(\beta) \equiv \frac{f(\beta)}{f(\beta_1)}, \tag{16}$$

where $f(\beta)$ is the two-loop scaling function of the SU(3) gauge theory, c_n's are parameters to describe deviation from the two-loop scaling, and β_1 is a reference point. Choosing $\beta_1 = 2.4$, the parameters

$$c_0 = 0.5443(97), \qquad c_2 = 0.390(38), \qquad c_4 = 0.049(12) \tag{17}$$

reproduce the measured values well.

III. RENORMALIZATION CONSTANTS

A. Results at Simulation Points

Calculations of Z-factors do not present any difficulty from $\beta = 8.0$ down to 2.6 for all lattice sizes, and at $\beta = 2.4$ and 2.2 on a small lattice of $4^3 \times 8$. For a larger $8^3 \times 16$ lattice at $\beta = 2.4$ and 2.2, however, we encounter "exceptional configurations." Deferring discussions of this issue, let us first summarize results for the nonexceptional case.

We first determine κ_c for each β and L/a. For this purpose simulations are carried out at several values of κ around an estimated κ_c in which m_q is determined by Eq. (10); we employ the fitting range given by $n = 0$ for $L/a = 4$ lattices, $n = 1$ for $L/a = 8$ lattices at $\beta = 2.4$ and 2.2, and $n = 2$ for $L/a = 8$ at other values of β and $L/a = 16$ lattices. We determine κ_c by a linear fit in κ as illustrated in Fig. 1 for an $8^3 \times 16$ lattice at $\beta = 2.6$.

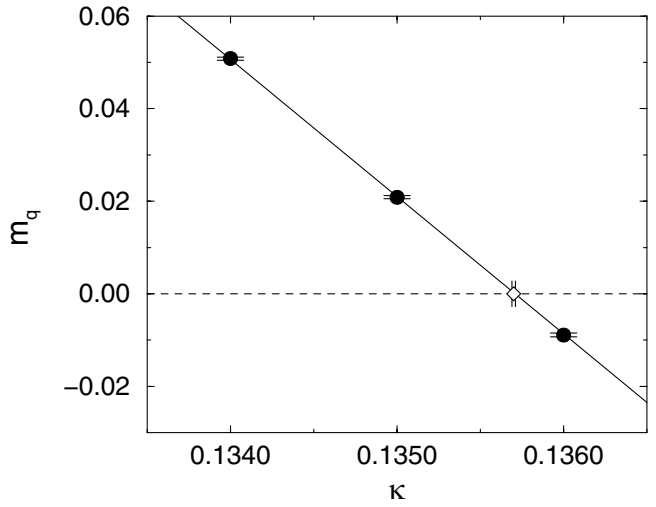

FIG. 1. m_q versus κ at $\beta = 2.6$ on an $8^3 \times 16$ lattice. Filled symbols show measured points. The open symbol represents κ_c.

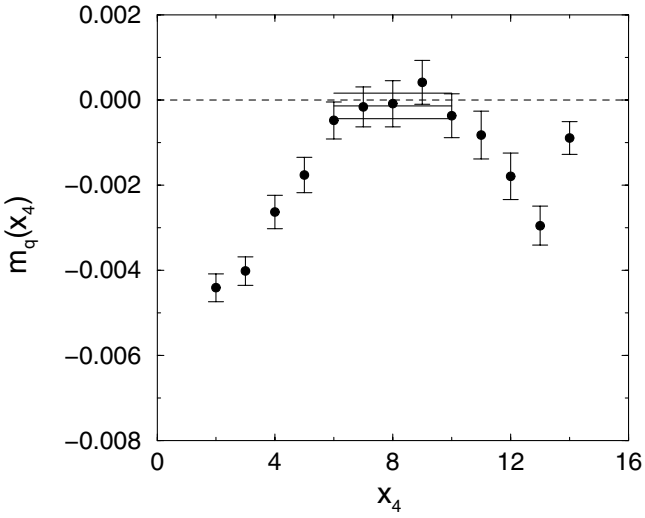

FIG. 2. Effective quark mass $m_q(x_4)$ at $\beta = 2.6$ on an $8^3 \times 16$ lattice. Horizontal solid lines represent fitting range, and fitted value and error.

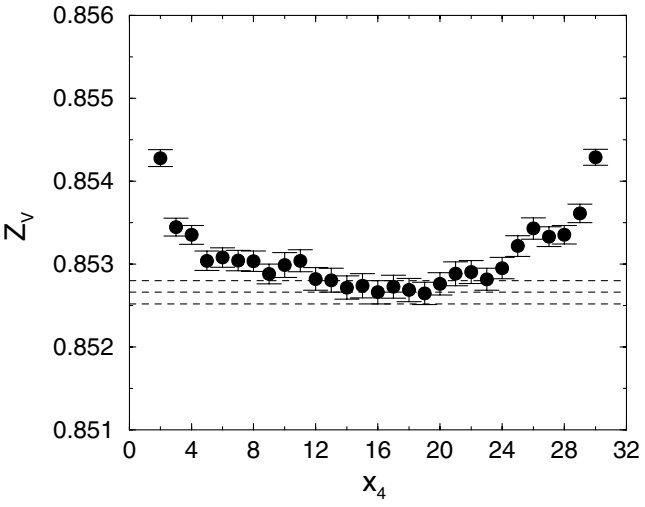

FIG. 3. Z_V as a function of time slice at $\beta = 3.125$ on a $16^3 \times 32$ lattice. Horizontal dashed lines represent Z_V at $x_4 = T/2 = 16$.

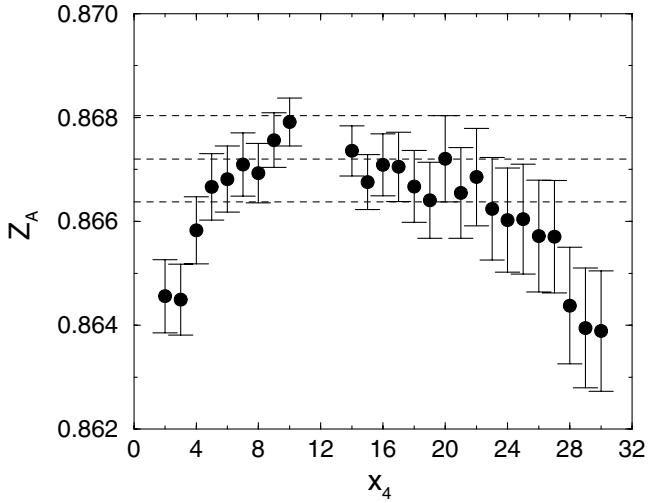

FIG. 4. Values of Z_A as a function of time slice at $\beta = 3.125$ on a $16^3 \times 32$ lattice. Horizontal dashed lines represent Z_A at $x_4 = (5/8) \cdot T = 20$.

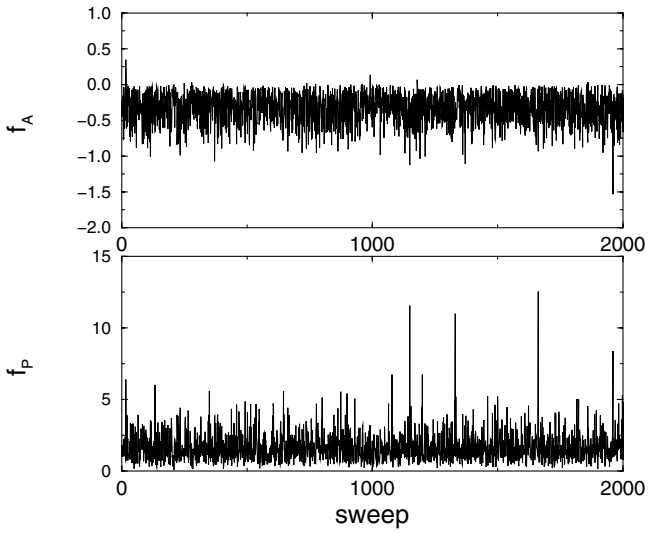

FIG. 6. Time history of f_A and f_P at $\beta = 2.6$ on an $8^3 \times 16$ lattice.

Results for κ_c are given in Table I. When we perform simulations for Z-factors at κ_c, m_q is also calculated for confirmation. A typical result for the effective quark mass $m_q(x_4)$ is shown in Fig. 2. It exhibits a reasonable plateau. Values of m_q at κ_c are given in the fourth column of Table I. They are consistent with zero within an accuracy of 10^{-3} at worst. Since κ_c is tuned well, errors of κ_c are not taken into account in the error estimation of Z-factors.

Figs. 3 and 4 show typical plots of Z_V and Z_A as a function of time slice. We observe good plateaux for all cases, except for a small temporal lattice size of $L/a = 8$ at strong coupling of $\beta = 2.4$ and 2.2. We thus find that the SF method works successfully for our action, albeit there are $O(ag^4)$ errors rather than $O(a^2)$ errors. Results for Z-factors at simulation points are given in Table I.

We now discuss the issue of "exceptional configurations." Among our parameter sets, anomalously large values appear in the ensemble of hadron correlators on an $8^3 \times 16$ lattice at $\beta = 2.4$ and 2.2. We illustrate the situation in Fig. 5, where we plot the time history of f_A and f_P at $\beta = 2.4$. No large spikes appear for larger β on the same size lattice, as shown in Fig. 6 for data at $\beta = 2.6$. Note that a much finer vertical scale is employed in the latter figure. Large spikes appear also in the ensembles of f_1, f_V and f_{AA} necessary for evaluating Z-factors. Such exceptional configurations make it difficult to determine m_q, κ_c and Z-factors precisely.

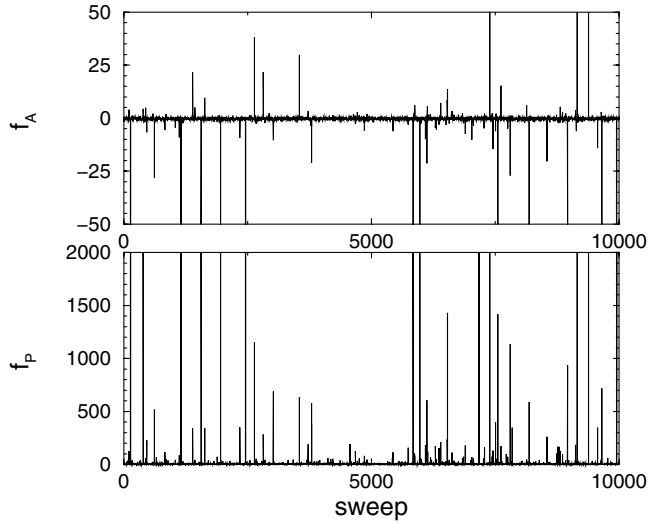

FIG. 5. Time history of f_A and f_P at $\beta = 2.4$ on an $8^3 \times 16$ lattice.

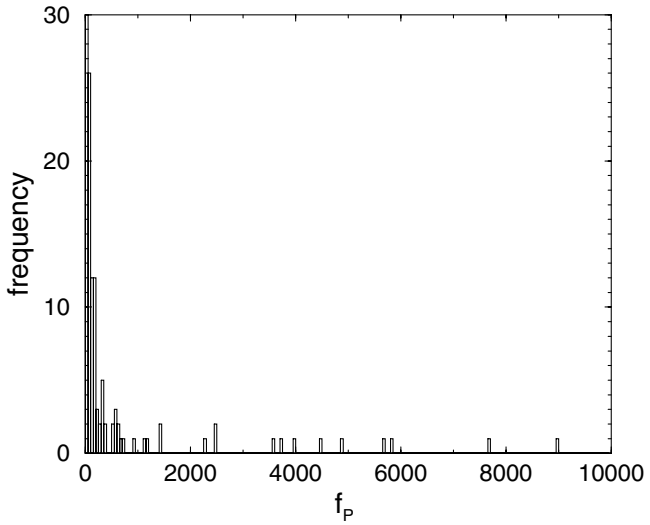

FIG. 7. Histogram of f_P at $\beta = 2.4$ on an $8^3 \times 16$ lattice. Intervals in x-axis are 50.

We suspect that the spikes are caused by the appearance of very small or even negative eigenvalues of the Dirac operator toward strong coupling. Such eigenvalues would be suppressed in full QCD by the quark determinant, and in this sense we expect exceptional configurations to be an artifact of quenched QCD. In quenched QCD, however, "exceptional configurations" cannot be distinguished from "normal" ones on some rigorous basis. In fact, histograms of f's have a long tail toward very large values as shown in Fig. 7. We then adopt the strategy of estimating Z-factors by removing from the ensemble average configurations having values above some cutoff. The uncertainties associated with this procedure are estimated by varying the cutoff, and will be propagated to systematic errors of Z-factors at fixed physical volume. Detailed description of this procedure will be given in Sec. III C.

B. Z-factors at Fixed Physical Volume

We plot Z_V and Z_A determined for various sizes and β in Figs. 8 and 9, respectively, as a function of a/L. There are three or four data points at $\beta = 8.0$ and 2.8 for Z_V, and at $\beta = 2.8$ for Z_A. These data show a linear behavior in a/L, which is consistent with the expectation that Z-factors for our action have $O(ag^4/L)$ errors. Therefore we adopt a linear ansatz to extrapolate or interpolate Z-factors to the physical volume of $L = 0.8$ fm (normalized at $\beta = 2.6$ and $L/a = 8$) and to $L = \infty$, as shown in these figures. We denote Z-factors at a fixed physical volume as $Z_{V,A}^{SF,L=0.8\text{fm}}$ and $Z_{V,A}^{SF,L=\infty}$. Numerical values are given in Table II.

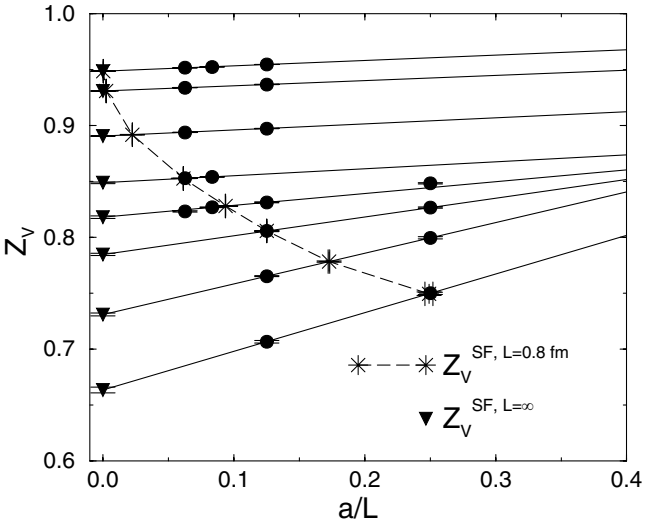

FIG. 8. Volume dependence of Z_V. Filled circles and solid lines are measured data and linear fits to them. Values of β are, from top to bottom, 8.0, 6.0, 4.0, 3.125, 2.8, 2.6, 2.4 and 2.2, respectively. Stars $Z_V^{SF,L=0.8\,\text{fm}}$ are connected by dashed lines to guide eyes. Filled triangles at $a/L = 0$ are $Z_V^{SF,L=\infty}$.

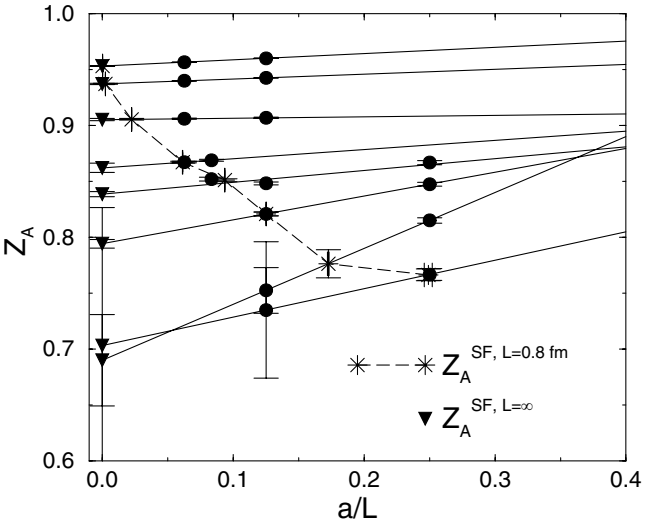

FIG. 9. Volume dependence of Z_A. Symbols are the same as in Fig. 8.

In Fig. 10 we plot Z_V as a function of g^2. Making a Padé fit, we obtain

$$Z_V^{SF,L=0.8\text{ fm}} = \frac{1 - 0.302\,225g^2 + 0.011\,034g^4}{1 - 0.239\,431g^2}, \quad (18)$$

$$Z_V^{SF,L=\infty} = \frac{1 - 0.365\,802g^2 + 0.015\,016g^4}{1 - 0.303\,008g^2}, \quad (19)$$

where we have imposed a constraint that the Padé fits reproduce the one-loop perturbative result $Z_V = 1 - 0.062\,794g^2$ [16] up to $O(g^2)$.

The range of coupling where there are data for the vector meson decay constant is marked by the two vertical dashed lines in Fig. 10. Over this range, $Z_V^{SF,L=\infty}$ becomes increasingly smaller (by about 8%–21%) compared to the one-loop value (dashed line) and the tadpole-improved value (crosses). We also observe that Z_V exhibits a sizable volume dependence toward strong coupling, *e.g.,* for $\beta \leq 2.8$. This will have an important consequence on the scaling property of f_ρ as discussed in Sec. IV.

TABLE II. Z-factors at fixed physical volumes.

β	$Z_V^{SF,L=0.8\text{fm}}$	$Z_V^{SF,L=\infty}$	$Z_A^{SF,L=0.8\text{fm}}$	$Z_A^{SF,L=\infty}$
2.2	0.7495(15)	0.6635(26)	0.7664(52)	0.7033(1221)
2.4	0.7783(05)	0.7309(13)	0.7763(127)	0.6900(409)
2.6	0.8056(05)	0.7847(11)	0.8208(18)	0.7942(39)
2.8	0.8279(02)	0.8180(12)	0.8511(13)	0.8386(22)
3.125	0.8526(01)	0.8488(07)	0.8671(08)	0.8621(42)
4.0	0.8917(02)	0.8904(03)	0.9055(08)	0.9052(10)
6.0	0.9309(02)	0.9308(02)	0.9372(05)	0.9371(05)
8.0	0.9485(01)	0.9485(01)	0.9530(03)	0.9530(03)

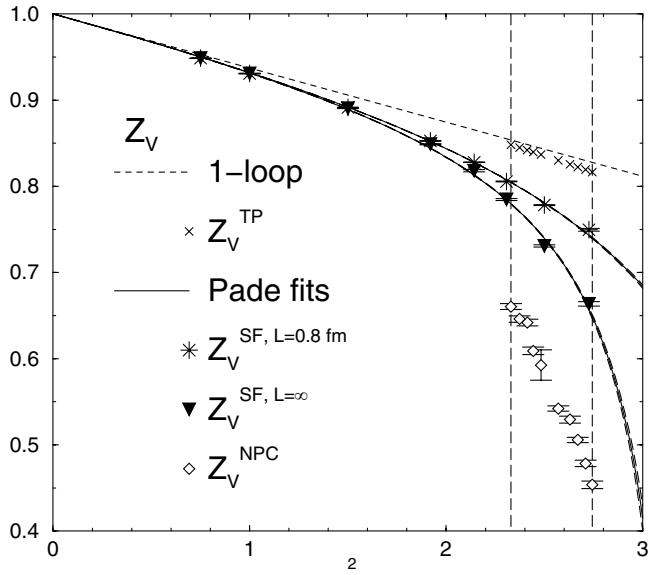

FIG. 10. Comparison of Z_V from tadpole-improved perturbation theory and those from SF method normalized at $L = 0.8$ fm and $L = \infty$. $Z_V^{\rm NPC}$ are determined with the conserved current. Padé fits and error are also given for Z_V from the SF method. Vertical dashed lines represent the range we have data for decay constants.

Another method to estimate Z_V nonperturbatively [17] utilizes the nonrenormalizability of the conserved vector current

$$V_i^C(x) = \frac{1}{2}\{\overline{\psi}(x + a\hat{\mu})U_{x,\mu}^{\dagger}(\gamma_i + 1)\psi(x) + \overline{\psi}(x)U_{x,\mu}(\gamma_i - 1)\psi(x + a\hat{\mu})\}, \quad (20)$$

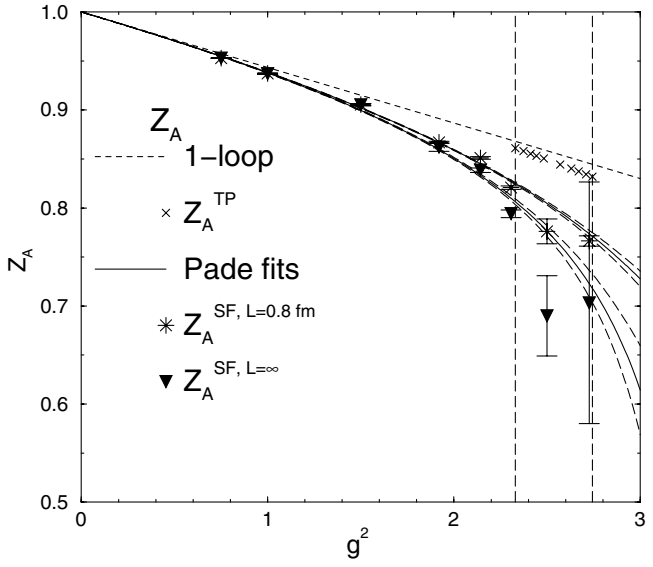

FIG. 11. Comparison of Z_A determined by various methods. Symbols are the same as in Fig. 10.

and defines

$$Z_V^{\rm NPC} = \lim_{x_4 \to \infty} \frac{\sum_{\mathbf{x}} \langle 0|V_i^C(\mathbf{x}, x_4)V_i|0\rangle}{\sum_{\mathbf{x}} \langle 0|V_i(\mathbf{x}, x_4)V_i|0\rangle}. \quad (21)$$

Results for $Z_V^{\rm NPC}$ obtained for our action combination [1] are also overlaid in Fig. 10 (open diamonds). They are much smaller than those from the SF method. We interpret that the large difference originates from large $O(a)$ errors in $Z_V^{\rm NPC}$. From the viewpoint of $O(a)$ improvement of operators, the divergence of a tensor operator $\partial_\mu T_{i\mu}$ should be added to both the local current V_i and the conserved current V_i^C [18]. However, the improvement operator $\sum_j \partial_j T_{0j}$, necessary for V_0 in the SF scheme, automatically drops out since it is a spatial total divergence. In other words, Z_V from the SF method is $O(a)$ improved, whereas $Z_V^{\rm NPC}$ is not.

In Fig. 11, we plot results for Z_A and Padé fits which read

$$Z_A^{SF,L=0.8\ {\rm fm}} = \frac{1 - 0.277\,576g^2 + 0.008\,669g^4}{1 - 0.220\,946g^2}, \quad (22)$$

$$Z_A^{SF,L=\infty} = \frac{1 - 0.334\,232g^2 + 0.011\,710g^4}{1 - 0.277\,602g^2}. \quad (23)$$

In the Padé fits, we use a constraint from one-loop perturbation theory that $Z_A = 1 - 0.056\,630g^2 + O(g^4)$ [16]. We observe that $Z_A^{SF,L=\infty}$ for the range we have data for f_π are smaller than the tadpole-improved value by 6%–14%.

C. Systematic Error from Exceptional Configurations

Exceptional configurations affect Z-factors in two ways, first by changing the value of m_q and hence of κ_c, and secondly by directly affecting the value of Z-factors themselves. Hence, in order to estimate the uncertainties

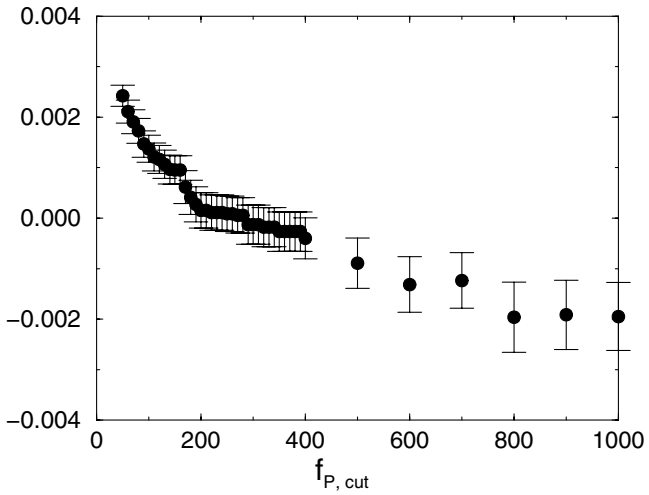

FIG. 12. m_q vs $f_{P,\rm cut}$ at κ_c on an $8^3 \times 16$ lattice at $\beta = 2.4$.

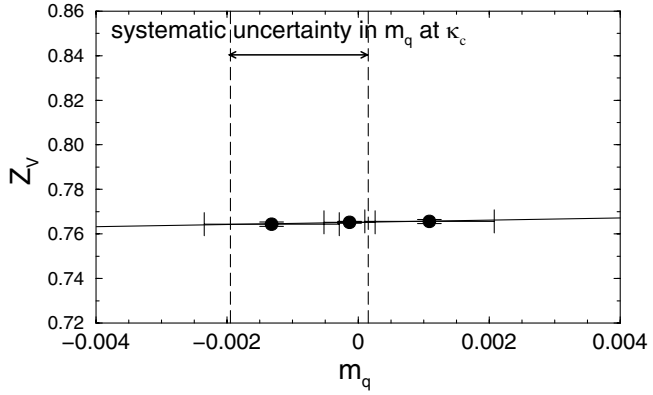

FIG. 13. Z_V versus m_q at $\beta = 2.4$ on an $8^3 \times 16$ lattice.

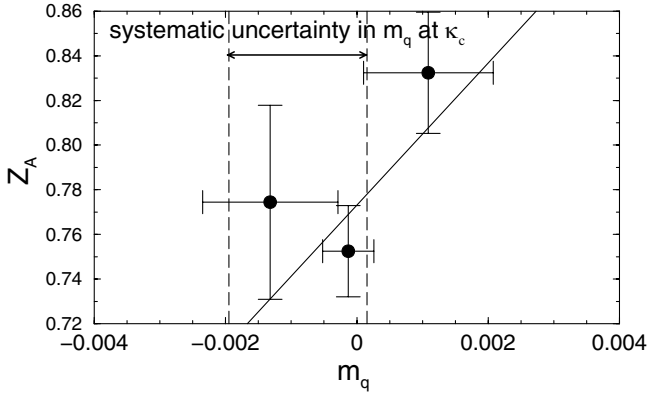

FIG. 14. Z_A versus m_q at $\beta = 2.4$ on an $8^3 \times 16$ lattice.

of Z-factors due to exceptional configurations at large couplings, we investigate how m_q and Z-factors change if we discard configurations having values of relevant correlators larger than some cutoff.

Figure 12 shows this test for m_q at $\beta = 2.4$ for which a cutoff is set for the value of f_P. As the cutoff $f_{P,\mathrm{cut}}$ is increased, m_q gradually decreases, becomes almost stable around $f_{P,\mathrm{cut}}$=300 and then the error of m_q becomes large. With this observation in mind, we have estimated κ_c as the point where m_q for $f_{P,\mathrm{cut}}$=300 is consistent with zero, as shown in Fig. 12. The uncertainty in m_q at κ_c is estimated by varying $f_{P,\mathrm{cut}}$ from 200 to 1000 and turns out to be $+0.00028 > m_q > -0.00182$. The same procedure at $\beta = 2.2$ with $f_{P,\mathrm{cut}}$=500 gives the uncertainty $+0.00344 > m_q > -0.00170$. We note that the number of configurations discarded is 37 (191) of the total of 10 000 (20 000) configurations at $\beta = 2.4$ (2.2).

The uncertainty of m_q is translated into uncertainties of Z-factors. To do this, we carry out two additional simulations at κ's slightly above and below κ_c. Figs. 13 and 14 show how Z-factors depend on m_q; Z_V is very stable against variation of m_q, while Z_A shows a more prominent dependence. We fit the m_q dependence of the Z-factors by a linear function, and uncertainties of Z-factors are estimated by the difference of the central value and the maximum/minimum value for the range of error of m_q. The uncertainties are given in Table III under the column δZ^{m_q}.

We also estimate uncertainties in the statistical averaging of Z-factors themselves by varying the cutoff of f_1. Figure 15 shows the ensemble average of f_1 and f_V together with Z_V as a function of the cutoff $f_{1,\mathrm{cut}}$. Though both f_1 and f_V increase as $f_{1,\mathrm{cut}}$, their ratio Z_V is very stable around $f_{1,\mathrm{cut}} = 5.0$ reflecting the fact that f_1 and f_V are highly and positively correlated. We determine the central value from $f_{1,\mathrm{cut}} = 5.0$ and estimate errors by varying $f_{1,\mathrm{cut}} = 2.0$ to 10.0. Figure 16 shows a similar test for Z_A. The cutoff dependence is more conspicuous than for Z_V. Uncertainties thus estimated are listed in Table III under the column $\delta Z^{\mathrm{except.}}$. Note that we discard 47 (221) configurations at $\beta = 2.4$ (2.2).

The two uncertainties δZ^{m_q} and $\delta Z^{\mathrm{except.}}$ are simply added to estimate the total uncertainty δZ for $L/a = 8$ lattices. We then propagate them to uncertainties of Z-factors at fixed physical volume, listed in Table III. Uncertainties at $L = 0.8$ fm are smaller than those on $L/a = 8$ lattices, because the physical size is located between $L/a = 8$ and $L/a = 4$ lattices. Uncertainties of Z-factors at $L = \infty$, enlarged by extrapolations, are larger than the statistical error $\delta Z^{\mathrm{stat},L=\infty}$.

D. Z-factors at Simulation Points for Meson Decay Constants

For discussions of scaling properties of meson decay constants, we need Z-factors at β values where raw data of f_ρ and f_π are taken. We evaluate them using the Padé fits obtained in Sec. III B together with the estimates of uncertainties from exceptional configurations.

For the latter purpose, we repeat Padé fits varying the Z-factor at $\beta = 2.4$ within the range of its uncertainty,

TABLE III. Breakdown of systematic uncertainties in Z-factors. See text for details.

	δZ^{m_q}	$\delta Z^{\mathrm{except.}}$	δZ	$\delta Z^{SF,L=0.8\mathrm{fm}}$	$\delta Z^{SF,L=\infty}$	$\delta Z^{\mathrm{stat},L=\infty}$
$Z_V(\beta = 2.2)$	+0.04%, −0.02%	+0.31%, − 0.06%	+0.35%, − 0.08%	+0.0013%, − 0.0058%	+0.75%, − 0.17%	0.39%
$Z_V(\beta = 2.4)$	+0.01%, − 0.12%	+0.08%, − 0.03%	+0.09%, − 0.15%	+0.044%, − 0.10%	+0.19%, − 0.31%	0.18%
$Z_A(\beta = 2.2)$	+3.2%, − 1.5%	+18.1%, − 2.1%	+21.3%, − 3.6%	+0.17%, − 0.25%	+44.5%, − 8.9%	17%
$Z_A(\beta = 2.4)$	+0.6%, − 8.0%	+6.1%, − 7.3%	+6.7%, − 15.3%	+4.0%, − 9.2%	+14.6%, − 33.4%	5.9%

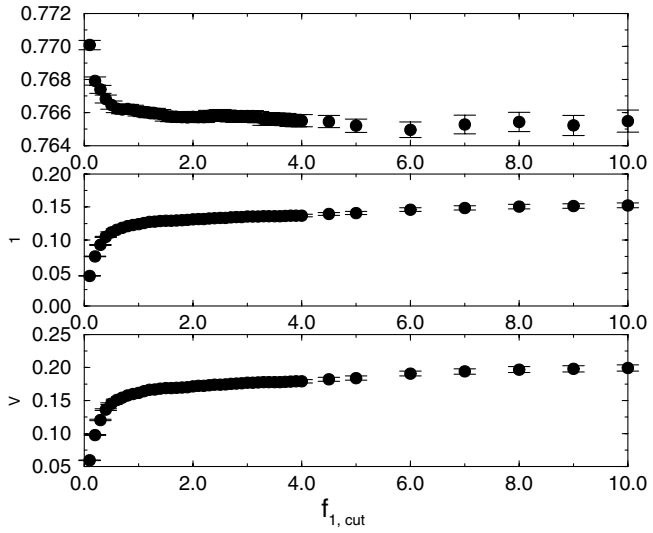

FIG. 15. Ensemble averages of f_1, f_V and Z_V versus $f_{1,\mathrm{cut}}$ at $\beta = 2.4$ on an $8^3 \times 16$ lattice.

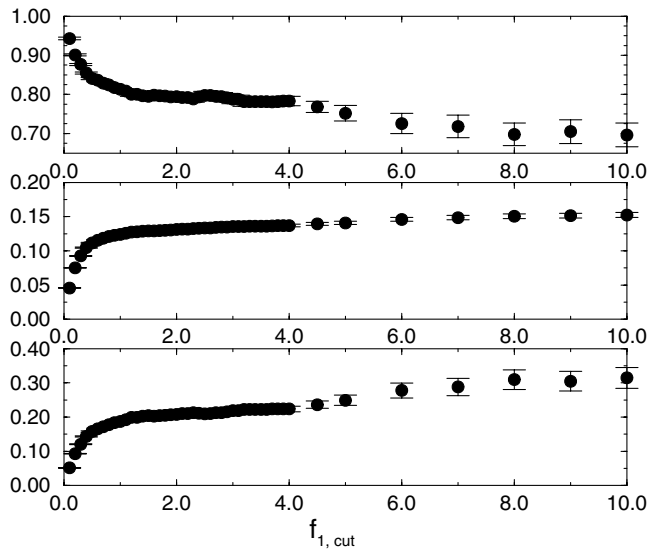

FIG. 16. Ensemble averages of f_1, f_{AA} and Z_A versus $f_{1,\mathrm{cut}}$ at $\beta = 2.4$ on an $8^3 \times 16$ lattice.

calculate the Z-factor at a target β value, and take the difference between this value and the central value as an estimate of the systematic error from exceptional configurations at $\beta = 2.4$. The systematic error from those at $\beta = 2.2$ is estimated similarly and added linearly to obtain the total systematic error.

Our final results for Z-factors at the simulation points for meson decay constants are listed in Table IV. The systematic errors in $Z_V^{SF,L=\infty}$ and $Z_A^{SF,L=\infty}$ are comparable to the statistical ones and within at most two σ. The ratio of systematic errors to statistical ones in the table is slightly smaller than the ratio at simulation points for Z-factors, $\beta = 2.4$ and 2.2, because the Padé fits are stabilized with data at $\beta \geq 2.6$ where no exceptional configurations appear. In the table, we reproduce the one-loop tadpole-improved values $Z_{V,A}^{TP}$ together with Z_V^{NPC} for comparison.

IV. SCALING PROPERTIES OF MESON DECAY CONSTANTS

We investigate the scaling property of f_ρ, combining the unrenormalized values of f_ρ [1] and four different choices of Z_V; 1) one-loop tadpole-improved value, Z_V^{TP}, 2) values determined by the SF method for $L = 0.8$ fm, $Z_V^{SF,L=0.8\ \mathrm{fm}}$, 3) those at $L = \infty$, $Z_V^{SF,L=\infty}$, and 4) Z_V^{NPC} in Eq. (21) defined by the conserved current. The unrenormalized f_ρ was determined in Ref. [1] for unimproved current. Hence, the renormalized f_ρ has $O(ag^2)$ error.

Numerical values of the renormalized f_ρ are listed in Table V. Statistical errors in the unrenormalized f_ρ and in $Z_V^{SF,L=0.8\ \mathrm{fm}}$ or $Z_V^{SF,L=\infty}$ are added in quadrature, while systematic uncertainties for the latter are simply propa-

TABLE IV. Z-factors at simulation points for meson decay constants.

β	Z_V^{TP}	$Z_V^{SF,L=0.8\mathrm{fm}}$	$Z_V^{SF,L=\infty}$	Z_V^{NPC}	Z_A^{TP}	$Z_A^{SF,L=0.8\mathrm{fm}}$	$Z_A^{SF,L=\infty}$
2.187	0.81657	$0.7400(08)^{+04}_{-10}$	$0.6488(24)^{+48}_{-27}$	0.4536(044)	0.83204	$0.7712(38)^{+27}_{-54}$	$0.7180(146)^{+125}_{-236}$
2.214	0.81923	$0.7462(07)^{+04}_{-09}$	$0.6651(20)^{+40}_{-23}$	0.4784(038)	0.83449	$0.7762(34)^{+24}_{-49}$	$0.7276(127)^{+109}_{-203}$
2.247	0.82237	$0.7532(06)^{+03}_{-08}$	$0.6825(16)^{+32}_{-19}$	0.5056(030)	0.83737	$0.7819(30)^{+21}_{-43}$	$0.7383(108)^{+093}_{-171}$
2.281	0.82548	$0.7601(06)^{+03}_{-07}$	$0.6981(13)^{+26}_{-16}$	0.5293(040)	0.84022	$0.7875(27)^{+19}_{-38}$	$0.7482(092)^{+080}_{-143}$
2.334	0.83009	$0.7698(04)^{+02}_{-06}$	$0.7187(10)^{+20}_{-13}$	0.5421(030)	0.84446	$0.7956(22)^{+16}_{-31}$	$0.7619(073)^{+063}_{-111}$
2.416	0.83673	$0.7832(03)^{+02}_{-04}$	$0.7441(07)^{+13}_{-09}$	0.5925(177)	0.85057	$0.8068(17)^{+12}_{-23}$	$0.7797(052)^{+045}_{-076}$
2.456	0.83978	$0.7891(03)^{+01}_{-03}$	$0.7544(06)^{+10}_{-08}$	0.6090(043)	0.85336	$0.8118(15)^{+10}_{-20}$	$0.7873(045)^{+038}_{-064}$
2.487	0.84205	$0.7934(03)^{+01}_{-03}$	$0.7617(06)^{+09}_{-07}$	0.6420(038)	0.85546	$0.8155(14)^{+09}_{-18}$	$0.7927(040)^{+034}_{-056}$
2.528	0.84496	$0.7988(02)^{+01}_{-03}$	$0.7705(05)^{+07}_{-06}$	0.6460(038)	0.85813	$0.8201(12)^{+08}_{-15}$	$0.7994(034)^{+029}_{-047}$
2.575	0.84816	$0.8046(02)^{+01}_{-02}$	$0.7796(05)^{+06}_{-05}$	0.6604(034)	0.86107	$0.8250(11)^{+07}_{-13}$	$0.8064(029)^{+024}_{-039}$

TABLE V. f_ρ and f_π in GeV with various choices of Z-factors.

β	a^{-1}[GeV]	$f_\rho(Z_V^{TP})$	$f_\rho(Z_V^{SF,L=0.8\text{fm}})$	$f_\rho(Z_V^{SF,L=\infty})$	$f_\rho(Z_V^{\text{NPC}})$	$f_\pi(Z_A^{TP})$	$f_\pi(Z_A^{SF,L=0.8\text{fm}})$	$f_\pi(Z_A^{SF,L=\infty})$
2.187	1.017(10)	0.2861(44)	$0.2593(43)^{+01}_{-04}$	$0.2273(43)^{+17}_{-09}$	0.1578(37)	0.1623(42)	$0.1504(46)^{+05}_{-11}$	$0.1401(65)^{+24}_{-46}$
2.214	0.966(10)	0.2761(38)	$0.2515(37)^{+01}_{-03}$	$0.2242(38)^{+13}_{-08}$	0.1601(32)	0.1555(37)	$0.1446(41)^{+04}_{-09}$	$0.1356(56)^{+20}_{-38}$
2.247	0.917(09)	0.2706(37)	$0.2478(36)^{+01}_{-03}$	$0.2246(36)^{+11}_{-06}$	0.1656(31)	0.1512(41)	$0.1412(44)^{+04}_{-08}$	$0.1333(56)^{+17}_{-31}$
2.281	0.896(10)	0.2704(38)	$0.2490(37)^{+01}_{-02}$	$0.2287(36)^{+09}_{-05}$	0.1723(33)	0.1423(33)	$0.1334(36)^{+03}_{-06}$	$0.1267(45)^{+14}_{-24}$
2.334	0.829(08)	0.2601(30)	$0.2412(29)^{+01}_{-02}$	$0.2252(29)^{+06}_{-04}$	0.1689(27)	0.1462(41)	$0.1377(42)^{+03}_{-05}$	$0.1319(50)^{+11}_{-19}$
2.416	0.734(09)	0.2471(54)	$0.2313(51)^{+01}_{-01}$	$0.2197(50)^{+04}_{-03}$	0.1744(78)	0.1368(39)	$0.1298(40)^{+02}_{-04}$	$0.1254(44)^{+07}_{-12}$
2.456	0.674(06)	0.2332(44)	$0.2191(42)^{+00}_{-01}$	$0.2095(41)^{+03}_{-02}$	0.1683(44)	0.1444(39)	$0.1374(40)^{+02}_{-03}$	$0.1332(44)^{+06}_{-11}$
2.487	0.652(07)	0.2467(42)	$0.2324(40)^{+00}_{-01}$	$0.2232(40)^{+03}_{-02}$	0.1874(40)	0.1358(36)	$0.1295(37)^{+01}_{-03}$	$0.1258(40)^{+05}_{-09}$
2.528	0.612(06)	0.2293(45)	$0.2168(43)^{+00}_{-01}$	$0.2091(42)^{+02}_{-02}$	0.1750(40)	0.1405(47)	$0.1343(47)^{+01}_{-02}$	$0.1309(49)^{+05}_{-08}$
2.575	0.574(06)	0.2417(37)	$0.2293(36)^{+00}_{-01}$	$0.2222(35)^{+02}_{-01}$	0.1872(34)	0.1445(53)	$0.1384(53)^{+01}_{-02}$	$0.1353(55)^{+04}_{-06}$

gated to that of the renormalized f_ρ. Fortunately, systematic uncertainties from exceptional configurations are sufficiently small. They are at most 0.4σ of the statistical errors and do not affect the conclusions below. Therefore we ignore systematic uncertainties in the following discussions.

Figure 17 presents the results for f_ρ as a function of a. Open circles are the previous result obtained with tadpole-improved one-loop Z-factor, which exhibits a sizable scaling violation. If instead one uses the nonperturbative Z_V for $L = \infty$, we observe a much better scaling behavior (filled triangles). The Z-factor evaluated for $L = 0.8$ fm lies in between the two results (stars).

We find this result very encouraging; it shows that an apparent large scaling violation seen with the use of Z_V^{TP} is largely due to neglecting higher order contributions in the Z-factor, and that inherent $O(a)$ errors in the vector decay constant are small even up to a large lattice spacing of $a^{-1} \sim 1$ GeV.

We extrapolate f_ρ with $Z_V^{SF,L=\infty}$ to the continuum limit linearly in a. The value in the continuum limit $f_\rho = 201.7(2.0)$ MeV turns out to be consistent with that $f_\rho = 205.7(6.6)$ MeV from a high precision simulation with the standard action [19].

We note that a relatively large scaling violation is observed for f_ρ with Z_V^{NPC} (open diamonds). Since f_ρ with Z_V^{NPC} is nothing but the decay constant determined from the conserved current in Eq. (20), we suspect that $O(a)$ large scaling violation exists in the conserved current.

The scaling property of f_π is investigated in a similar manner. We note that the unrenormalized f_π in Ref. [1] was determined for the improved current using a tadpole-

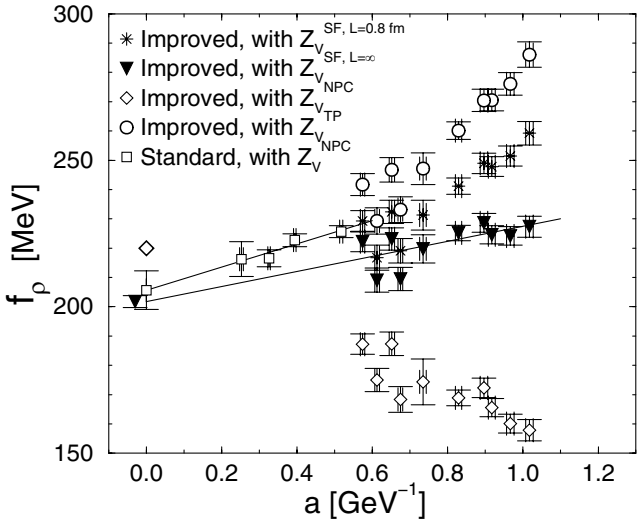

FIG. 17. f_ρ versus a with various choices of Z_V. Values for our improved action with Z_V^{TP} and Z_V^{NPC} are taken from Ref. [1]. Values for the standard action [19] are determined with Z-factors from the conserved current. Diamond at $a = 0$ represents the experimental value.

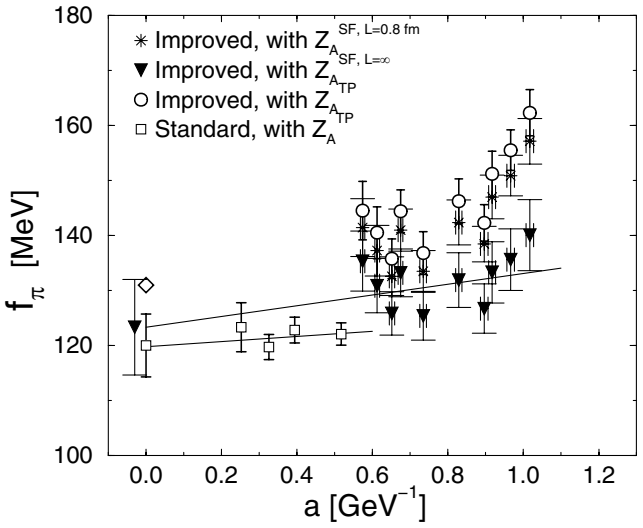

FIG. 18. f_π versus a with various choices of Z_A. Symbols are the same as in Fig. 17, though f_π from the standard action is determined with Z_A^{TP}.

improved one-loop value of c_A with $\overline{\mathrm{MS}}$ coupling, whereas Z-factors in this work employ c_A with bare coupling. The difference in the renormalized f_π arising from the difference of c_A remains $O(ag^4)$.

Figure 18 shows f_π versus a. In this figure, we have not included the systematic uncertainty since, being smaller than statistical one, it does not alter the conclusions below. Numerical values are listed in Table V. The conclusions on the scaling behavior are similar to those of f_ρ. Employing $Z_A^{SF,L=\infty}$, which includes terms to all orders in g^2 and does not have $O(ag^4/L)$ error, the scaling behavior turns out to be better than previous results with tadpole-improved one-loop Z-factor indicated. Making a linear continuum extrapolation, we obtain a value $f_\pi = 123.3(8.7)$ MeV consistent with that $f_\pi = 120.0(5.7)$ MeV calculated with the standard action at significantly weaker couplings (open squares).

V. CONCLUSIONS

The Schrödinger functional method has been applied to calculations of the vector and axial-vector renormalization constants for the combination of a RG-improved gauge action and a tadpole-improved clover quark action. With the Z-factors determined nonperturbatively, an apparent large scaling violation in the range of lattice spacing $a^{-1} = 1 - 2$ GeV in the meson decay constants previously observed with the one-loop perturbative Z-factors is significantly reduced. We conclude that the improvement attempted with the gluon and quark actions employed in the present work is effective for the meson decay constants as well.

We find that scaling of decay constants is best when one uses Z-factors normalized at infinite volume. This suggests that removing $O(ag^4/L)$ error in Z-factors by the limiting procedure $L \to \infty$ is important for actions with $O(ag^4)$ error.

The nonperturbative Z-factors have enabled us to determine values in the continuum limit of decay constants. We may expect that other hadronic matrix elements are also reliably extracted from lattice spacings much coarser than $a^{-1} \approx 2$ GeV for our action combination if one uses Z-factors determined by the Schrödinger functional method.

Finally we recall that a large scaling violation for the meson decay constants has been observed also in two-flavor full QCD with the same action combination of quenched QCD considered in this article. A nonperturbative determination of Z-factors will therefore be interesting to pursue for this case. Exceptional configurations are expected to be absent in full QCD. Therefore the Schrödinger functional calculation would be more straightforward. Work in this direction is in progress.

ACKNOWLEDGMENTS

This work is supported in part by Grants-in-Aid of the Ministry of Education (Nos. 12304011, 13135204, 13640260, 14046202, 14740173, 15204015, 15540251, 15540279, and 16028201).

[1] CP-PACS Collaboration, A. Ali Khan *et al.*, Phys. Rev. D **65**, 054505 (2002); **67**, 059901(E) (2003).
[2] Y. Iwasaki, Nucl. Phys. **B258**, 141 (1985); Y. Iwasaki, Univ. of Tsukuba Report No. UTHEP-118, (1983) (unpublished).
[3] G. P. Lepage and P. B. Mackenzie, Phys. Rev. D **48**, 2250 (1993).
[4] B. Sheikholeslami and R. Wohlert, Nucl. Phys. **B259**, 572 (1985).
[5] M. Lüscher, R. Narayanan, P. Weisz, and U. Wolff, Nucl. Phys. **B384**, 168 (1992).
[6] M. Lüscher, S. Sint, R. Sommer, and P. Weisz, Nucl. Phys. **B478**, 365 (1996).
[7] ALPHA Collaboration, M. Lüscher, S. Sint, R. Sommer, P. Weisz and U. Wolff, Nucl. Phys. **B491**, 323 (1997).
[8] ALPHA Collaboration, M. Lüscher, S. Sint, R. Sommer, and H. Wittig, Nucl. Phys. **B491**, 344 (1997).
[9] CP-PACS Collaboration, S. Aoki *et al.*, Nucl. Phys. B (Proc. Suppl.) **106**, 780 (2002).
[10] CP-PACS Collaboration, K. Ide *et al.*, Nucl. Phys. B (Proc. Suppl.) **129**, 426 2004.
[11] Y. Taniguchi and A. Ukawa, Phys. Rev. D **58**, 114503 (1998).
[12] S. Aoki, R. Frezzotti, and P. Weisz, Nucl. Phys. **B540**, 501 (1999).
[13] S. Takeda, S. Aoki, and K. Ide, Phys. Rev. D **68**, 014505 (2003).
[14] CP-PACS Collaboration, A. Ali Khan *et al.*, Phys. Rev. D **64**, 114501 (2001).
[15] C. R. Allton, hep-lat/9610016.
[16] S. Aoki, K. Nagai, Y. Taniguchi, and A. Ukawa, Phys. Rev. D **58**, 074505 (1998).
[17] L. Maiani and G. Martinelli, Phys. Lett. B **178**, 265 (1986).
[18] G. Martinelli, C. T. Sachrajda, and A. Vladikas, Nucl. Phys. **B358**, 212 (1991).
[19] CP-PACS Collaboration, S. Aoki *et al.*, Phys. Rev. Lett. **84**, 238 (2000); Phys. Rev. D **67**, 034503 (2003).